Photocatalytic Activity of TiO₂-Containing Nanocomposites versus the Chemical Nature of the Polymeric Matrices: A Comparison

Fabiana Vento, Angelo Nicosia,* Lidia Mezzina, Giulia Raciti, Antonino Gulino, Marcello Condorelli, Luisa D'Urso, Guido De Guidi, and Placido Mineo*

Environmental remediation of xenobiotic pollutants is an important issue in industrialized society. Catalyst-mediated pollutant photodegradation using solar light shows promising results. Titanium dioxide nanoparticles (TiO₂ NPs) are a well-known standard for mineralizing organic water pollutants. Its use as a sludge pointed out the need to support this photocatalyst to ease both its use and recovery. Polymers represent a viable solution because of their versatility, stability, and cheapness. The in situ radical bulk polymerization approach to the development of TiO₂-based thermoplastic nanocomposites for xenobiotic photodegradation enhances the photocatalytic performance of the semiconductor nanoparticles. The versatility and efficiency of these systems pave the way for their industrial applications as photocatalytic coatings for large-scale surfaces. To shed light on the influences of the chemical nature of the polymer matrix on the photocatalytic efficiency of the nanosystems, polyvinyl acetate, polymethyl methacrylate, and polystyrene are investigated as supports for TiO₂ NPs. The obtained TiO₂-containing nanocomposites are characterized by thermal analyses, UV-vis, Raman, and X-ray photoelectron spectroscopies, dynamic light scattering, and contact angle measurements. The photocatalytic activity of the nanosystems in the form of thin films is investigated against pollutants in water solutions, and shows clear differences in the photodegradation efficiency among the nanocomposites having different chemical natures of polymers.

F. Vento, A. Nicosia, L. Mezzina, G. Raciti, A. Gulino, M. Condorelli,
L. D'Urso, G. De Guidi, P. Mineo
Department of Chemical Sciences and INSTM UdR of Catania
University of Catania
V.le A. Doria 6, Catania 95125, Italy
E-mail: angelo.nicosia@unict.it; gmineo@unict.it
P. Mineo
Institute of Polymers
Composites and Biomaterials
National Research Council (IPCB-CNR)
Via P. Gaifami 18, Catania 95126, Italy

The ORCID identification number(s) for the author(s) of this article can be found under https://doi.org/10.1002/admt.202300391

1. Introduction

Xenobiotic pollution in aqueous and air environmental matrices is a major critical issue of the Anthropocene era.[1] Since the great acceleration that began during the industrial revolution, several new synthetic compounds (namely xenobiotics)[2] have been introduced into the environment,[3] causing ecological hazards and health risks. In this framework, the need to clean up vital resources has led to the development of several methods in recent years,[2] such as advanced oxidation processes. Among these, the photodegradation of pollutants triggered by solar light is considered the most promising approach, also due to the exploitation of a potentially infinite and green energy source.[4]

Titanium dioxide in the form of nanoparticles (TiO₂ NPs) is one of the most popular and promising heterogeneous photocatalysts for water remediation, due to its photoreactivity, chemical and physical stability, bioinertness, and low cost.[5] In particular, exploiting a synergistic effect between Anatase and Rutile phases, Degussa P-25 TiO₂ nanopowder was established as a standard in photocatalysis. Nevertheless, the main drawbacks of this system are due to the charge recombination and oxidation rates, which strongly decrease the efficiency of the photocatalyst.[6] Furthermore, its highest efficiency under UV illumination rather than visible light, due to its band gap value ($\approx$3 eV),[7] reflects the low adsorption and quantum efficiency, thus narrowing its application. To overcome these limitations, several modifications are currently under investigation, such as metal and non-metal doping,[7c,8] and coupling with other nanosystems.[9] In addition, the use of dye sensitizers[10] is a promising method for broadening light absorption into the visible light range. On the other hand, the development of three-dimensionally ordered porous TiO₂ NPs has shown improvements in light-absorption efficiency. This is attributed to a light-harvesting effect (arising from the increased optical path within the semiconductor macrostructure) that supports the efficient penetration of the incident photon flux into the

**ADVANCED
SCIENCE NEWS**

www.advancedsciencenews.com

**ADVANCED
MATERIALS
TECHNOLOGIES**

www.advmattechnol.de

photocatalytic porous nanoparticles.[11] Recently, a combined approach involving doping of porous TiO₂ macrostructures has also shown promising results in the mineralization of organic pollutants, both in liquid and gas phases.[12]

Nevertheless, the use of TiO₂ NPs as suspended powder points out the need to separate the catalyst from the depolluted fluids using expensive recovery treatments. Such an issue could be avoided by anchoring TiO₂ NPs on solid supports. In fact, several supports (glass, concrete, plastic, etc.) have already been investigated.[6] Unfortunately, the common approaches involve expensive procedures and methods, such as thermal treatments,[13] sol-gel approaches,[14] and vapor deposition techniques.[15] In this field, polymers are fascinating supports due to their chemical inertness, stability, and cheapness. Moreover, thermoplastic polymers can be easily turned into thin films and coatings, facilitating the use of the material in large-scale applications. Indeed, a photocatalytic coating that is easily applicable on surfaces could support the depollution of water and air matrices by exploiting sunlight. The simplest immobilization technique might be to blend TiO₂ NPs with a polymer using a proper solvent and to dry the mixture.[16] Nevertheless, embedding nanoparticles in a polymer matrix could reduce their available surface area and affect their photocatalytic efficiency.[17]

Recently, we have proposed a new in situ radical bulk polymerization approach to develop polymethyl methacrylate-based thermoplastic nanocomposites containing TiO₂ NPs.[18] This method ensures intimate contact between the monomers and the photocatalytic particles before the polymerization, which can affect the light transmission and charge separation efficiencies. The resulting nanocomposites have already shown promising results in the photocatalytic degradation of xenobiotic pollutants.[19]

Nevertheless, an investigation on the effects of the chemical nature of the used polymeric matrices with respect to the photocatalytic efficiency of the nanosystem has not been performed yet.

To shed light on the interactions between the polymer and the photocatalyst, and to understand potential side effects, different common polymeric matrices were investigated in this work: i) polyvinyl acetate (PVAc), a polymer frequently employed as a base in paints; ii) polymethyl methacrylate (PMMA), a material commonly used for optical applications; iii) polystyrene (PS), a cheap and widely used vinyl polymer applied as an insulator. The resulting nanocomposites were characterized by thermogravimetric analysis (TGA), differential scanning calorimetry (DSC), UV-vis, Raman and X-ray photoelectron spectroscopies, and dynamic light scattering (DLS). The wettability of the nanocomposite films was evaluated by contact angle measurements. The photocatalytic activity of the nanosystems in the form of thin films was investigated by batch experiments against pollutants in solution, determining the photodegradation rate of model dyes such as Methylene Blue and Rhodamine B. The collected data allowed a correlation between efficiency and polymeric chemical nature. To

show the effectiveness of the experimental nanosystems toward real air pollution, a canvas coated with photocatalytic nanocomposites was exposed for several months to a city environment (a busy road). The results showed, by simple optical observation, the excellent performance of the nanosystems, evidencing a different photodegradation efficiency between the polymeric matrices. The cheap synthetic procedure and the stability of the nanocomposite organic solution make it a promising material for a potential industrial scale-up.

2. Results and Discussion

Aiming to investigate the effects of different polymer matrices on the performances of thermoplastic-based nanocomposite photocatalysts, three different nanocomposites having different polymeric matrices were synthesized.

A one-pot synthesis was developed by exploiting an in situ radical polymerization (see **Figure 1**). Briefly, a suitable monomer (Methyl Methacrylate, Vinyl Acetate, or Styrene) and TiO₂ NPs (5% w) were mixed by prolonged sonication, allowing the adsorption of the monomer inside TiO₂ NPs pores. Subsequently, the thermal initiator (2,2'-Azo-bisisobutyronitrile) was added, and the mixture was then heated at 55 °C for 20h. Finally, the unreacted monomer and unwanted oligomers were removed by precipitation in *n*-hexane.

The photooxidation capability of the nanocomposites is strictly related to the amount of TiO₂ NPs entrapped within. Hence, to determine the TiO₂ NPs content in each nanocomposite, thermogravimetric analyses were performed in the air (see **Figure 2** and the table therein). In this oxidative atmosphere, the PMMA and PS homopolymers showed single-step degradation beginning at approximately 270 and 350 °C, respectively, due to both unzipping and oxidative processes. Instead, PVAc showed a multi-step thermal degradation ($T_1 = 314$ °C, $T_2 = 426$ °C, $T_3 = 485$ °C) determined by deacetylation and further oxidative processes.[20] Due to the presence of nanoparticles within the polymer matrix, PMMA@TiO₂ and PS@TiO₂ showed higher thermal stability and residues than the related homopolymers (PMMA@TiO₂: T = 340 °C; residue at 800 °C: 4.87%; PS@TiO₂: T = 380 °C; residue at 800 °C = 4.89%). Furthermore, the multi-step degradation of PVAc was slightly shifted to higher temperatures after the addition of the photocatalyst nanoparticles ($T_1 = 319$ °C, $T_2 = 424$ °C, $T_3 = 507$ °C, with a residue of 5.11% at 800 °C).

The differences between the nominal loading of TiO₂ (w%) and its real content within the nanocomposites are due as a consequence of both the polymer fully conversion and the nanocomposites purification steps: the removal of unreacted monomers and the suspended hybrid species determine a slightly different TiO₂ content than the nominal one.

Glass transition temperatures (Tg) obtained by DSC analyses showed negligible differences between homopolymers (**Figure 3**, dashed lines) and their related nanocomposites (Figure 3,
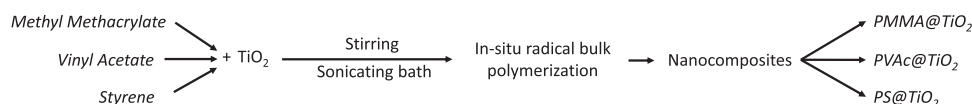

Figure 1. Simplified scheme for the synthesis of the nanocomposites with different polymeric matrices.
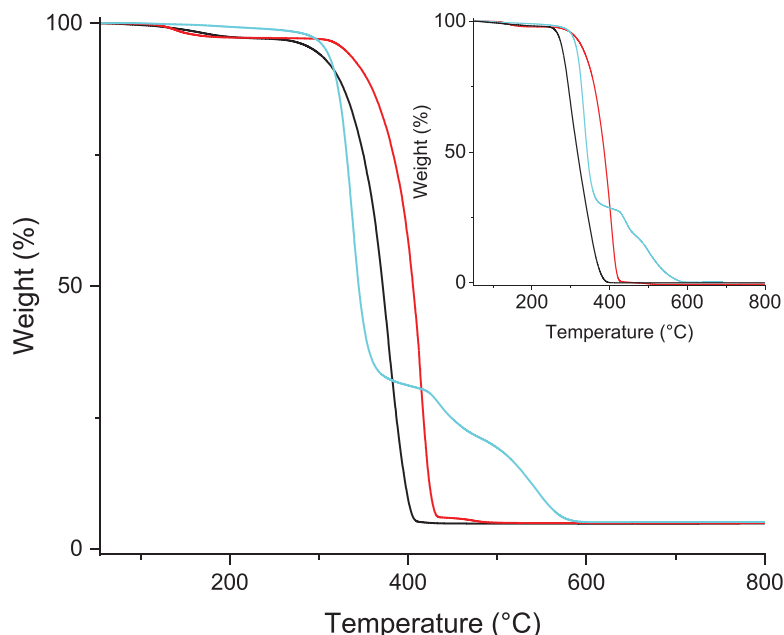
**ADVANCED
SCIENCE NEWS**

www.advancedsciencenews.com

**ADVANCED
MATERIALS
TECHNOLOGIES**

www.advmattechnol.de

Sample	Degradation T * (°C)	Residue at 800 °C (w %)
PMMA	273	0
PMMA@TiO$_2$	339	4.87
PS	348	0
PS@TiO$_2$	377	4.89
PVAc	314 426 485	0
PVAc@TiO$_2$	319 424 507	5.11

* Degradation temperatures are reported as onset temperature of the weight loss step

Figure 2. TGA traces (air atmosphere) of PMMA@TiO$_2$ (black line), PVAc@TiO$_2$ (cyan line), and PS@TiO$_2$ (red line). Inset shows the TGA traces of the homopolymers PMMA (black line), PVAc (cyan line), and PS (red line). The degradation step temperatures and the residue values at 800°C are reported in the table.

continuous lines). Thus, it could be assumed that the nanoparticles embedded within the polymer matrix do not affect the organization of the polymer chains in the solid state.

As a confirmation of the intimate contact between the organic matrix and the semiconductor nanoparticles, the storage of the nanocomposites' THF suspensions does not result in precipitation phenomena or phase separation also after a month of storage.[18] On the contrary, the dispersion of TiO$_2$ NPs within a solvent suffers precipitation after a few minutes, as well as its blended mixture with the polymers.

The capability of the nanocomposites to increase the dispersibility of the embedded nanoparticles was further confirmed by DLS analysis performed on the THF suspensions of the nanocomposites. The data showed a high scattering intensity in the range centered at about 100 nm (**Figure 4**), which is in agreement with the nominal size of the TiO$_2$ NPs and further confirms the negligibility of eventual self-aggregation processes.

The band gap energy of the samples was estimated through the modified Kubelka-Munk function F(R) as a function of the photon energy (hν). For what concerns the homopolymers, the optical properties are listed in Figure 5c.
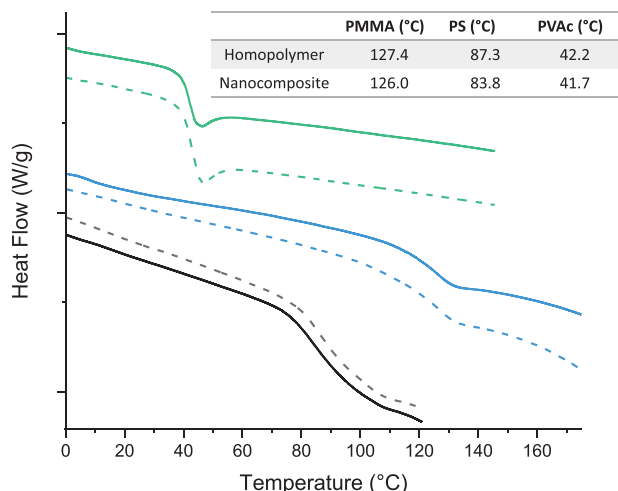

	PMMA (°C)	PS (°C)	PVAc (°C)
Homopolymer	127.4	87.3	42.2
Nanocomposite	126.0	83.8	41.7

Figure 3. DSC traces of PVAc@TiO$_2$ (green solid line), PMMA@TiO$_2$ (blue solid line), PS@TiO$_2$ (black solid line), PVAc (green dashed line), PMMA (blue dashed line) and PS (black dashed line). The calculated glass transition temperatures are reported in the inset table.
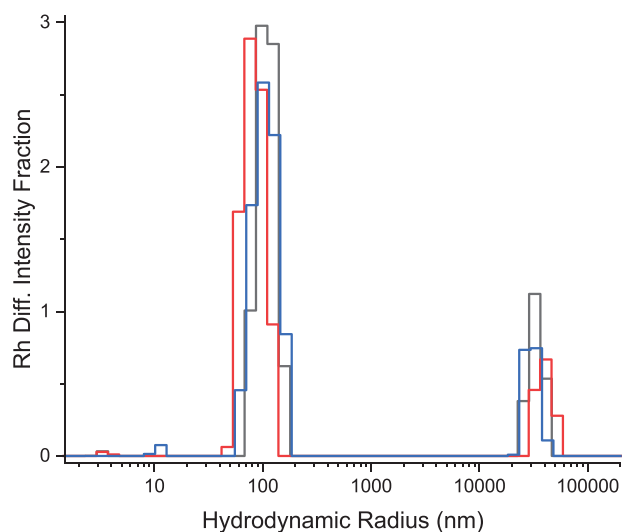

Figure 4. DLS traces of THF solutions of PMMA@TiO$_2$ (black), PS@TiO$_2$ (red), and PVAc@TiO$_2$ (blue).

**ADVANCED
SCIENCE NEWS**

www.advancedsciencenews.com

**ADVANCED
MATERIALS
TECHNOLOGIES**

www.advmattechnol.de

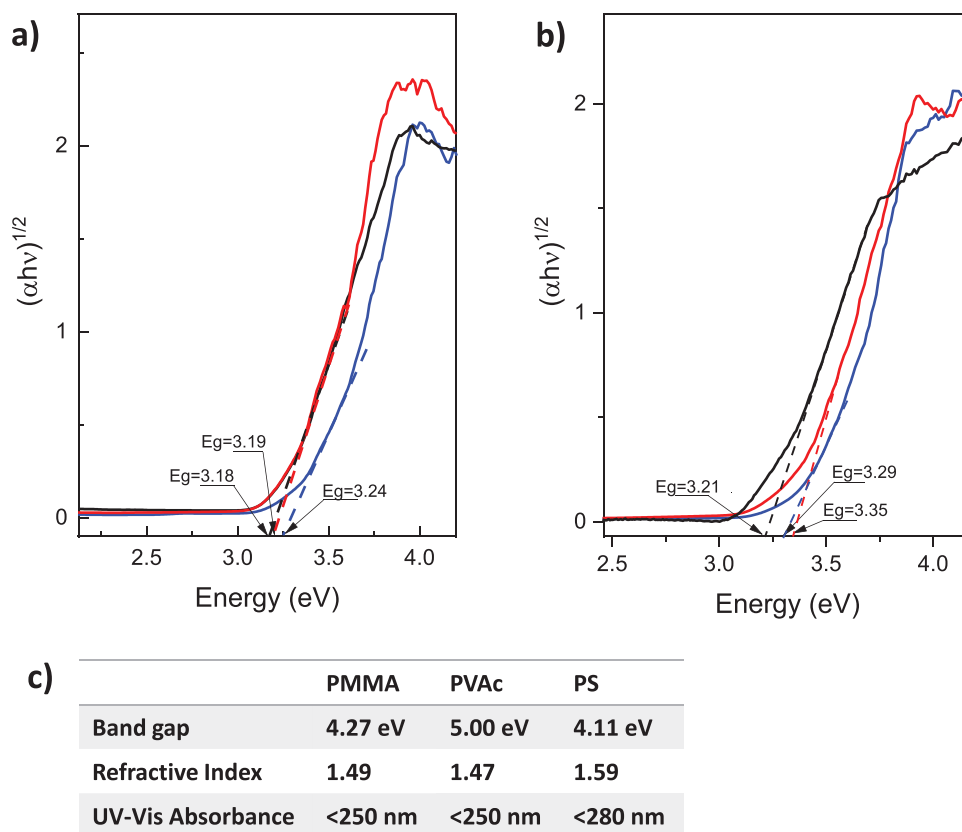| c)		PMMA	PVAc	PS
Band gap		4.27 eV	5.00 eV	4.11 eV
Refractive Index		1.49	1.47	1.59
UV-Vis Absorbance		<250 nm	<250 nm	<280 nm

Figure 5. Diffuse Reflectance spectra of a) blends PMMA-TiO_2 (black line), PS-TiO_2 (red line), and PVAc (blue line); b) nanocomposites PMMA@TiO_2 (black line), PS@TiO_2 (red line) and PVAc@TiO_2 (blue line); c) The Table reports the optical properties of the homopolymer films.[22]

The bandgap of the samples shows a slight change from the value of bare TiO_2 (3.20 eV)[21] due to the interaction with the polymer matrix. The extrapolated band gap values of the blends (**Figure 5**a) are 3.24 eV for PVAc-TiO_2, 3.19 eV for PMMA-TiO_2, and 3.18 eV for PS-TiO_2; meanwhile, those of nanocomposites (Figure 5b) are 3.29 eV for PVAc@TiO_2, 3.21 eV for PMMA@TiO_2, and 3.35 eV for PS@TiO_2. Nevertheless, the slight differences between these bandgap values are negligible, and likely within the error of the method.

The crystallographic structure of TiO_2 NPs, including the presence of defects or lattice distortions, was investigated by Raman spectroscopy. The positions of characteristic peaks of TiO_2 Anatase crystalline structure are well known in the literature,[23] having six Raman active fundamental modes: 144 cm^{-1} (E_{g1}), 197 cm^{-1} (E_{g2}), 397 cm^{-1} (B_{1g}), 518 cm^{-1} (A_{1g}) and 640 cm^{-1} (E_{g3}). The analysis by Raman spectroscopy coupled with the 2D Raman imaging map gives powerful and detailed spectral information about the spatially resolved chemical composition and crystalline structure of nanocomposite materials. Thus, each nanocomposite was deposited by drop casting onto a silicon substrate and imaging maps were recorded, obtaining the intensity maps of the peak at 144 cm^{-1}, which is the most intense vibration of Anatase (brighter zones), while dark areas are mainly composed of polymer (**Figure 6**). To highlight the effect of different preparation methods of polymer-TiO_2 composites on the distribution of nanoparticles within the polymer matrix, imaging maps of the corresponding blend mixtures were also collected.

In general, the chemical maps of the nanocomposite polymer@TiO_2 films (Figure 6a,c,e) revealed that the TiO_2 NPs, represented by the bright yellow spots, are more homogeneously distributed than those of the blended samples (Figure 6b,d,f), without any phase separation phenomenon of the catalyst from the polymer. This observation was further confirmed by the Raman spectra recorded in bright and dark regions of the nanocomposites and blend films. The spectra of the nanocomposites films showed always the E_{g1} mode at 144 cm^{-1} in both bright (Figure 6g) and dark (Figure 6h) regions, confirming the homogeneous dispersion of TiO_2 in the polymer matrix.

In contrast, the Raman maps of the polymer-TiO_2 blends show segregation phenomena of TiO_2 NPs within the polymer matrices, minor for PVAc-TiO_2 blend (Figure 6d), and particularly evident for PMMA-TiO_2 and PS-TiO_2 blends (Figure 6b,f, respectively), as demonstrated by the large bright yellow areas surrounded by areas devoid of catalyst. The Raman spectra obtained from the two different bright and dark zones (Figures 6g,h, respectively) for each sample confirmed this statement. It is widely reported that Raman spectral features (Raman shift, linewidth, and peak symmetry) are strongly dependent on crystal size, because of the spatial confinement of phonons in metal oxide crystallites.[24] Specifically, the peak E_{g1} should show a low-frequency shift (red) and a significant narrowing with the increase in the TiO_2 crystallite size. Focusing on the size distribution of the catalyst nanoparticles, although all of the investigated
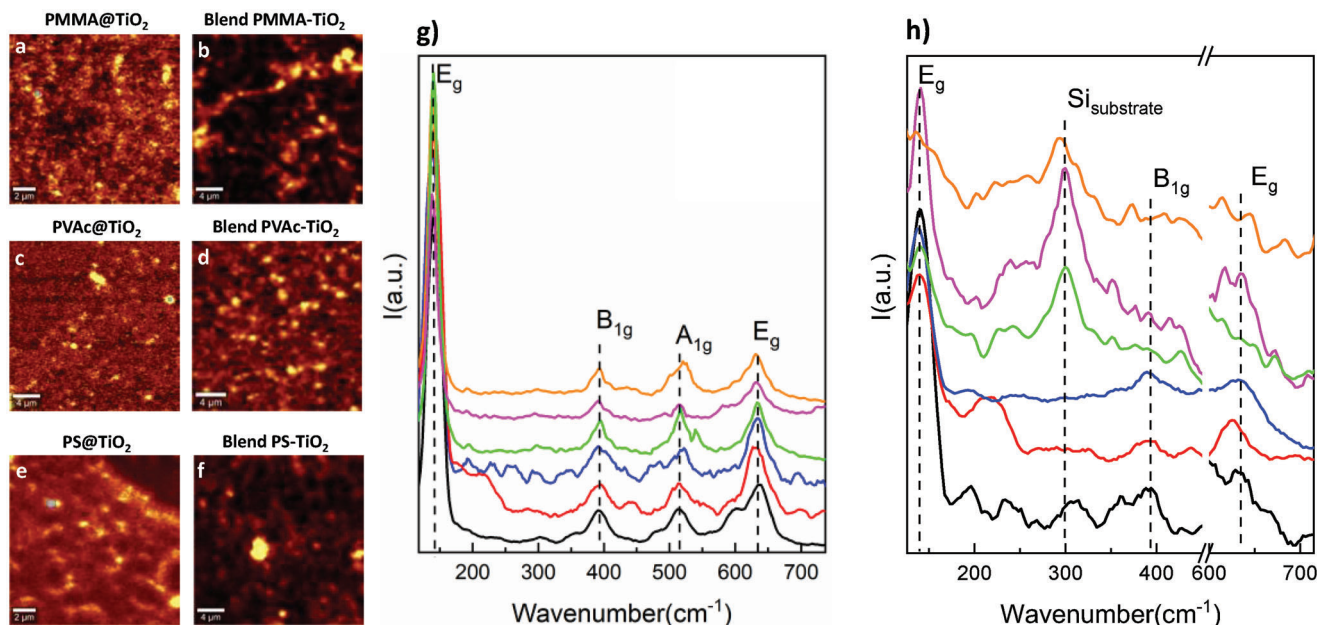
Figure 6. Raman imaging maps of nanocomposites and blended mixture counterparts: PMMA@TiO$_2$ a) and blend PMMA-TiO$_2$ b), PVAc@TiO$_2$ c) and blend PVAc-TiO$_2$ d), PS@TiO$_2$ e) and blend PS-TiO$_2$ f). Raman spectra of bright g) and dark h) regions of PMMA@TiO$_2$ (black line) and blend PMMA-TiO$_2$ (green line), PVAc@TiO$_2$ (blue line), and blend PVAc-TiO$_2$ (orange line), PS@TiO$_2$ (red line) and blend PS-TiO$_2$ (magenta line).

blends show extended TiO$_2$ NPs rich regions, we did not observe any changes in the Raman spectra. In fact, both the recorded E_{g1} frequency and the extrapolated line width (FWHM) value remain unchanged respectively at ≈144 and 197 cm^{-1}, suggesting no relevant change in the Anatase nanoparticles size as a result of phase segregation phenomena.

The electronic structure of the best performing PMMA@TiO$_2$ nanocomposite (vide infra) was studied by XPS analyses and results were compared with those of the bare TiO$_2$ NPs. The inelastic mean free path λ for the Ti 2p core level electrons is 12.5 Å and the separation between adjacent Ti-containing planes in the (110) main direction for TiO$_2$ NPs is 3.24 Å.[25] Since XPS is a surface technique that probes just a maximum depth corresponding to 3 λ, ≈11 ionic planes can be investigated.

Figure 7 shows the XPS spectra of the commercial TiO$_2$ NPs sample (black line) and that of PMMA@TiO$_2$ (red line), in the Ti 2p energy region. The Ti 2p feature of the commercial sample consists of the main 2p$_{3/2}$, 2p$_{1/2}$ spin-orbit components at 459.2 and 465.0 eV, respectively. Upon inclusion in PMMA, we noted very low-intensity Ti 2p XPS signals and a 0.1 eV shift of both spin-orbit components at higher energy with a concomitant band broadening. This band broadening is mainly due to the low-intensity signals of the TiO$_2$ NPs now included in the PMMA pores and to some polymer C-Ti interactions. There are no evident color changes nor additional XPS evidence of low binding energy peaks and this fact suggests the substantial absence of TiO$_2$-x species on the XPS probed depth being the 459.2 and 465.0 eV values typical of the TiO$_2$ NPs itself.[25b,26] In fact, the eventual presence of Ti$_2$O$_3$ species, in which the Ti ions are in a 3+ valence state, should give origin to an XPS spectrum consisting of a pair of overlapping Ti 2p doublets (with the new doublet due to Ti^{3+} at lower binding energy) because of the competition of various final state screening effects.[27]

Figure 8 shows the XPS spectra of the commercial TiO$_2$ NPs sample (black line) and that of PMMA@TiO$_2$ (red line), in the C 1s binding energy region. The peak at 285.0 eV is due to the adventitious carbon contamination present in all air-exposed materials and the weak signal at 288.6 eV is due to a few carbonates on the surface of the commercial TiO$_2$ NPs sample. In the case of PMMA@TiO$_2$, the peak at 285.0 eV is due to the PMMA aliphatic groups, and the last signal, now at 288.9 eV, significantly increased upon the TiO$_2$ NPs inclusion in the polymer, is mainly due to the -COOR group of the PMMA.

The XPS of the O 1s core level of the same samples is shown in **Figure 9**. The commercial TiO$_2$ NPs show a strong signal at
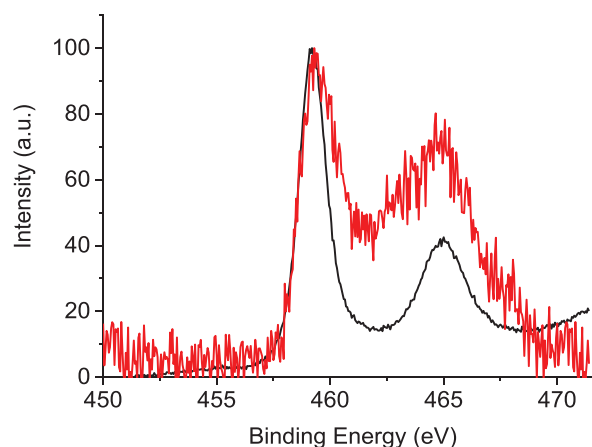

Figure 7. Al Kα excited XPS of the commercial TiO$_2$ sample (black line) and PMMA@TiO$_2$ (red line) in the Ti 2p binding energy region. Structures due to Al Kα satellites were removed from the spectra. The spectra were normalized to the same relative intensity.
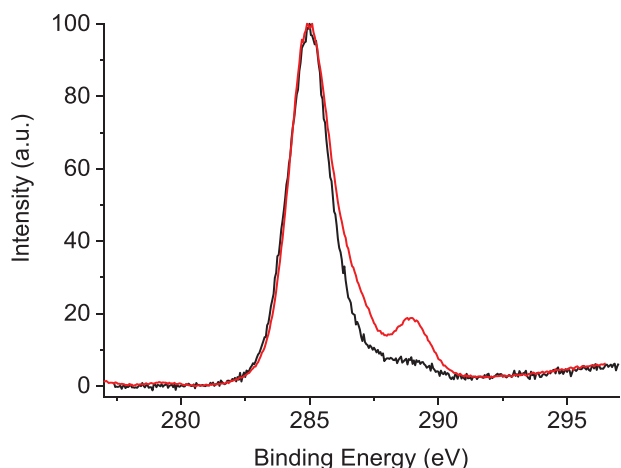
**ADVANCED
SCIENCE NEWS**

www.advancedsciencenews.com

**ADVANCED
MATERIALS
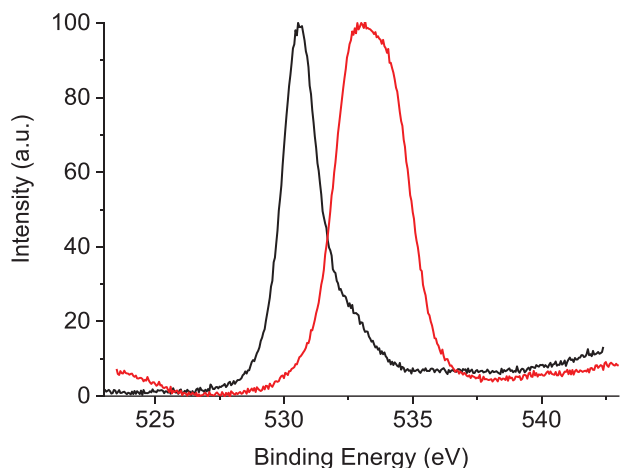TECHNOLOGIES**

www.advmattechnol.de

Figure 8. Al Kα excited XPS of the commercial TiO_2 NPs sample (black line) and PMMA@TiO_2 (red line) measured in the C 1s binding energy region. Structures due to Al Kα satellites were removed from the spectra. The spectra were normalized to the same relative intensity.

530.6 eV, as expected for TiO_2 materials, with a high energy, low-intensity tail due to the presence of some Ti-OH hydroxide on the sample surface.[25b] In contrast, XPS of PMMA@TiO_2 shows a broad O 1s peak centered at 533.0 eV due to the two oxygen atoms of the -COOR group of PMMA and to some relevant presence of surface water responsible of the ≈535 eV component.

The photocatalytic efficiency of the nanocomposites was verified through batch photo-oxidation experiments involving model dyes and real pollutants (**Figures** 10 and 11).

The adsorption of the dyes onto the polymer-based system was considered through preliminary dark storage under stirring (Figure 10c). The photodegradation experiments of Methylene Blue (**Figure 10**a, continuous lines; Figure 10d) revealed only a little higher efficiency of the PMMA@TiO_2 and PVAc@TiO_2 nanocomposites (normalized k equal to 14.20 and 15.17 $min^{-1}g^{-1}$, respectively) with respect to the PS@TiO_2 counterpart (normalized k 12.29 $min^{-1}g^{-1}$). Instead, considering the

photodegradation experiments of Rhodamine B (Figure 10b,d), the PMMA@TiO_2 system has shown the best performance (normalized k 5.61 $min^{-1}g^{-1}$). On the contrary, each physical mixture of PMMA, PVAc, or PS with TiO_2 NPs, under the same experimental conditions, has shown low efficiency (Figure 10a, dashed lines).[18]

To confirm the stability and reusability of the nanocomposites, each thin film was used for three photodegradation cycles of both Methylene Blue (inset in Figure 10a) and Rhodamine B (inset in Figure 10b). After each photocatalytic cycle, the thin films were copiously washed with water (LC-MS grade) to remove any residual adsorbed dye and/or intermediate species. The experiments revealed a decrease of normalized k of ≈1% per cycle.

The photodegradation efficacy of our nanosystems was also scrutinized against two common classes of environmental pollutants (pesticides, e.g. Methyl Viologen also named Paraquat, and drugs, e.g. Acetaminophen) in an aqueous solution. Variations in the concentration of pollutants, obtained by monitoring the bands at 243 nm (Acetaminophen) and 257 nm (Paraquat), were reported in **Figure 11**a,b, respectively.

The data highlighted the highest efficacy of the PMMA@TiO_2 nanosystem against both pollutants (Table in Figure 11). Instead, the PVAc@TiO_2 nanosystem was active only against Acetaminophen. On the other hand, the PS@TiO_2 nanosystem showed the lowest efficiency in all experiments.

These behaviors could be explained by considering the different chemical natures of the polymer matrices and/or their interaction with the photocatalyst and the solvent/pollutant.

In particular, the surface wettability of the nanocomposite might be a key parameter, as heterogeneous photocatalytic degradation of organic molecules is a surface process that takes advantage of the presence of water to induce the production of the hydroxyl radical species.[19] Contact angle experiments (Figure 12) showed that the wettability of the three examined nanocomposites (PMMA@TiO_2, PVAc@TiO_2, and PS@TiO_2) increased in the PS<PMMA<PVAc sequence (97.6°, 80.1° and 77.4°, respectively).

On the other hand, the wettability is strongly dependent on the chemical structure of the polymer, and the low wettability of the PS matrix is due to the polymer chemical structure containing hydrophobic benzene moieties that, in turn, reduces the water adsorption and thus its photocatalytic efficiency. Instead, in the cases of PVAc and PMMA matrices, despite the PVAc showing a slightly higher wettability, the better photocatalytic performance of the PMMA matrix may be due to a better carry of photons into the porosity of the PMMA@TiO_2 system.[28]

Finally, as a proof of concept of the efficiency of photocatalytic nanocomposites also towards air pollution in a real city environment, the nanocomposites (PS@TiO_2, PVAc@TiO_2, and PMMA@TiO_2) were used as ink to write the word "SMOG" by brushing the same amount of their dispersion in THF onto a white canvas (**Figure 13**, left-bottom). As a reference, related homopolymers free of TiO_2 NPs were also used for the same purpose (Figure 13, left-top).

The canvas was exposed in an open environment in front of the busy ring road of the city of Catania (Italy) for 9 months (May-January) in a sunny position. When evaluating the canvas after 9 months, as expected, altered colors of the canvas due to the effects of pollution were observed. Nevertheless,
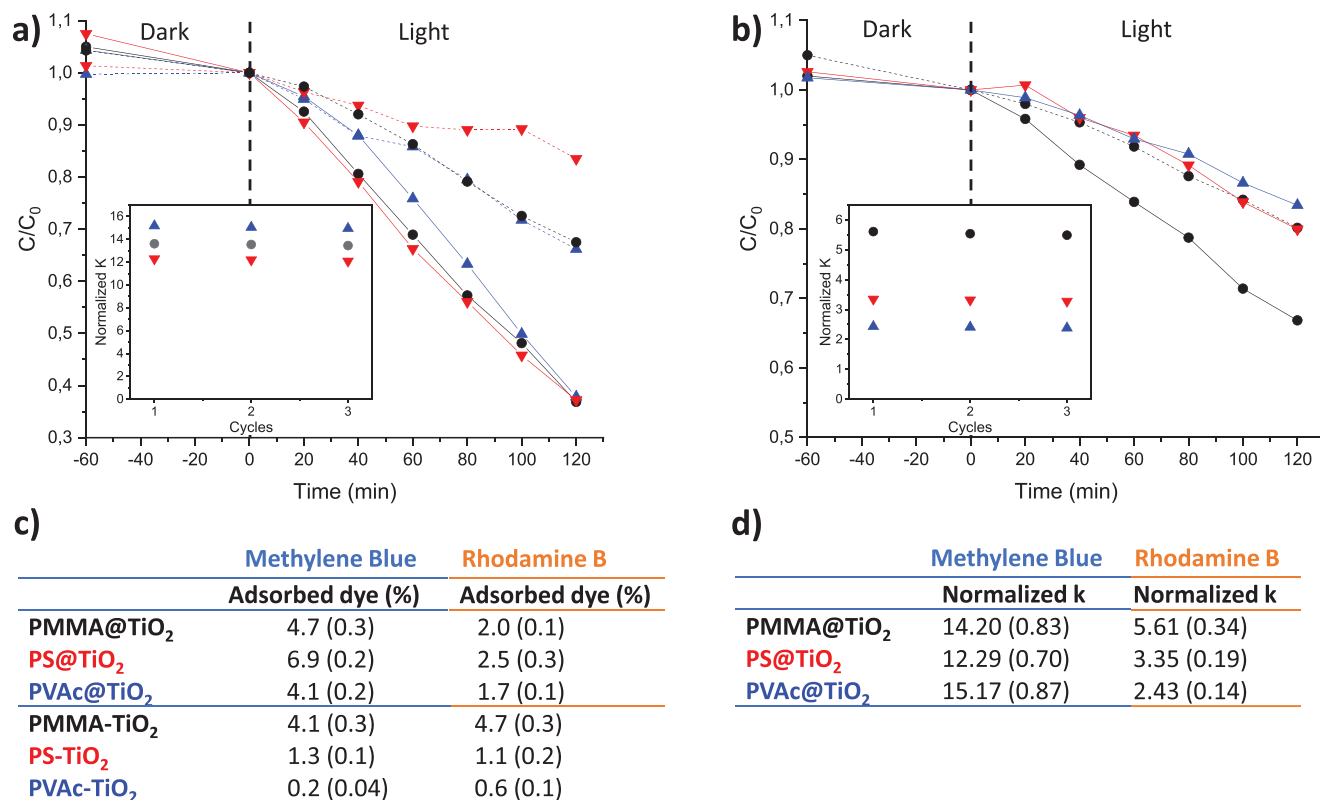

Figure 9. Al Kα excited XPS of the commercial TiO_2 NPs sample (black line) and PMMA@TiO_2 (red line) measured in the O 1s binding energy region. The spectra were normalized to the same relative intensity.

Figure 10. Methylene Blue a) and Rhodamine B b) photodegradation in the presence of nanocomposites (continuous lines) and blended mixtures (dashed lines) thin films. Each polymer matrix is reported with a different color: black for PMMA, red for PS, and blue for PVAc. Inset: normalized rate constant for the weight of the catalyst obtained during the reuse of each nanocomposite thin film with Methylene Blue and Rhodamine B, respectively. The tables show, respectively: c) the adsorbed dye amount (%mol) with different nanocomposite and blends during the dark storage time, and d) the normalized k for each photodegradation experiment (the standard deviation errors are reported in the brackets). The normalized k represents the kinetic constant normalized by the weight of the active photocatalyst.

c)

	Methylene Blue	Rhodamine B
	Adsorbed dye (%)	Adsorbed dye (%)
PMMA@TiO$_2$	4.7 (0.3)	2.0 (0.1)
PS@TiO$_2$	6.9 (0.2)	2.5 (0.3)
PVAc@TiO$_2$	4.1 (0.2)	1.7 (0.1)
PMMA-TiO$_2$	4.1 (0.3)	4.7 (0.3)
PS-TiO$_2$	1.3 (0.1)	1.1 (0.2)
PVAc-TiO$_2$	0.2 (0.04)	0.6 (0.1)

d)

	Methylene Blue	Rhodamine B
	Normalized k	Normalized k
PMMA@TiO$_2$	14.20 (0.83)	5.61 (0.34)
PS@TiO$_2$	12.29 (0.70)	3.35 (0.19)
PVAc@TiO$_2$	15.17 (0.87)	2.43 (0.14)

the areas covered with the photocatalytic nanocomposites maintained the original bright white color of the canvas, thus showing "SMOG" words brighter white for PMMA@TiO$_2$ than PVAc@TiO$_2$ and PS@TiO$_2$ (Figure 13, bottom right). Instead, the canvas surface that had the same word written with the pure homopolymers did not reveal any bright areas (Figure 13, top right).

Finally, based on the bright intensity of the word "SMOG", the canvas experiment confirmed the highest photodegradation efficiency of the PMMA@TiO$_2$ nanosystems, showing a much more bright written. We want to stress that all nanocomposites have the same TiO$_2$ NPs dispersion homogeneity within the polymer matrix.

Therefore, to explain the highest efficiency of PMMA@TiO$_2$ over PVAc@TiO$_2$, different parameters must be taken into account, and the interactions of the organic matrix with the semiconductor nanoparticles should play a key role. It has been reported that, as well as the wettability, the PMMA matrix induces local waveguide effects of the light arising from differences in the material's refractive indexes,[29] that enhance the light propagation within the material. Finally, the electric dipole layer originated by the electronic charge interaction at the PMMA/TiO$_2$ interface might accelerate the charge separation more efficiently than in PVAc/TiO$_2$ or in PS/TiO$_2$.[30]

3. Conclusion

Present data indicate that different monomers could be used for in-situ radical bulk polymerization to produce TiO$_2$-containing nanocomposites. Such an approach would ensure the homogeneity of the TiO$_2$ NPs dispersion within the polymer matrix, despite the different nature of the monomers used. The growth of the polymer chains within the pores of the semiconductor photocatalyst nanoparticles, which is induced by the synthetic approach, might be responsible for the enhanced photocatalytic performances of the nanocomposites with respect to those of the related blended mixture.

Nevertheless, a combined influence from the optical properties of the polymer and the wettability of the matrix must be taken into account. Indeed, the PS@TiO$_2$ nanocomposite, which showed the lowest wettability, was also negligibly active against all the model pollutants in the water solution. On the other hand, the highest wettability of the PVAc@TiO$_2$ nanocomposites is reflected in its efficiency against a noncharged water pollutant such as Acetaminophen. However, the PMMA@TiO$_2$ showed the best photodegradation efficiency towards all the model pollutants used in this work, regardless of the chemical nature of the pollutant. This result may be attributed to the optical properties of the PMMA matrix that ensure a better photon carry effect into the
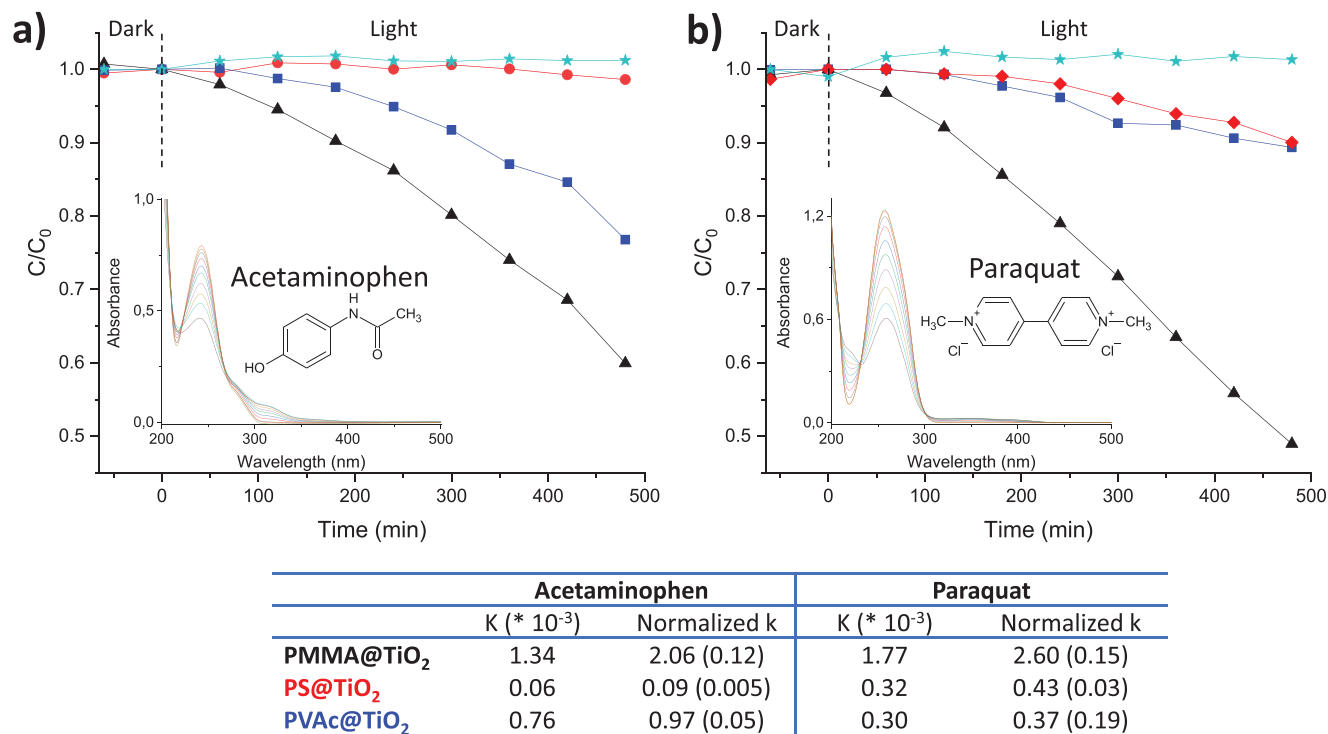
**ADVANCED
SCIENCE NEWS**

www.advancedsciencenews.com

**ADVANCED MATERIALS
TECHNOLOGIES**

www.advmattechnol.de

	Acetaminophen		Paraquat	
	K (* 10^{-3})	Normalized k	K (* 10^{-3})	Normalized k
PMMA@TiO$_2$	1.34	2.06 (0.12)	1.77	2.60 (0.15)
PS@TiO$_2$	0.06	0.09 (0.005)	0.32	0.43 (0.03)
PVAc@TiO$_2$	0.76	0.97 (0.05)	0.30	0.37 (0.19)

Figure 11. Photodegradation kinetics of Acetaminophen a) and Paraquat b) in the absence of photocatalyst (green), and with thin films of PS@TiO$_2$ (red), PVAc@TiO$_2$ (blue), and PMMA@TiO$_2$ (black). The insets show the UV-vis spectra of Acetaminophen and Paraquat acquired during photodegradation experiments employing PMMA@TiO$_2$. The table contains the normalized k for each photodegradation experiment (the standard deviation error is reported in the brackets).

photocatalyst nanoparticles that, in turn, boosts the photodegradation efficiency of the semiconductor. Moreover, this hypothesis is furtherly supported by the photodegradation experiments against air pollutants performed through a coated canvas, where the PMMA@TiO$_2$ confirmed its highest efficiency compared to the other polymer matrices. A favorable outlook for these materials is given with regard to their potential industrial scale-up. This possibility is strongly supported by the simple and cheap synthetic approach. Moreover, the versatility of the thermoplastic films allows them to be applied onto different surfaces exposed to sunlight, through conventional easy and inexpensive techniques, such as brushing or dipping.

4. Experimental Section

Methyl methacrylate, Vinyl acetate, Styrene, 2,2'-Azobisisobutyronitrile (AIBN), sodium sulfate, basic alumina, THF, *n*-hexane, water (LC-MS grade), titanium dioxide nanoparticles (Degussa P25, 21 nm primary particle size (TEM), 35–65 m^2 g^{-1} (BET)), Rhodamine B, Methylene Blue, Acetaminophen, and Methyl Viologen (Paraquat) were provided by Sigma–Aldrich.

Instruments: A Pyris TGA 7 supplied with a TAC 7/DX (Perkin Elmer) was used to perform thermogravimetric analyses, throughout a temperature range from 50 to 800 °C (heating rate 10 °C min^{-1}), and air flux (60 mL min^{-1}). Degradation temperatures were calculated as the Onset's point.

Differential scanning calorimetry (DSC) analyses were performed employing a DSC Q20 (TA Instruments) coupled with a Refrigerant Cooling System (heating rate 10 °C min^{-1}), and dry nitrogen flux (60 mL min^{-1}).

A Cary60 UV-vis spectrophotometer (Agilent Technologies) was used to acquire UV-vis spectra (temperature 25 ± 0.1°C, quartz cuvettes with 1 cm path length), using water as solvent.

Dynamic light scattering (DLS) measurements were performed with a miniDAWN Treos multi-angle light scattering detector equipped with a Wyatt QELS-DLS module (Wyatt Technology), and performing the data analysis with the ASTRA software (version 6.0.1.10, Wyatt Technology).

The crystalline phase of TiO$_2$ NPs and their dispersion homogeneity in the polymeric films were also investigated by analyzing Raman scattering data and Raman imaging maps obtained at 144 cm^{-1} (corresponding to the most intense vibrational signal of the Anatase phase). Raman spectra have been excited with a 532 nm laser line of a Coherent Compass Sapphire Laser (Coherent Inc., Santa Clara, CA, USA) mounted on a WITec alpha 300 (Wissenschaftliche Instrumente und Technologie GmbH, Ulm, Germany) confocal Raman apparatus. Spectra have been collected with a 50× objective (spot size of ≈2 μm).

Imaging maps were recorded to perform grid measurements (100 points and 100 lines) of 15 × 15 μm and 25 × 25 μm, obtaining images in false color in which bright spots are related to TiO$_2$ NPs, while dark areas are mainly composed of the polymer.

X-ray photoelectron spectra (XPS) were measured on the as-prepared samples at 45° take-off angles relative to the surface plane with a PHI
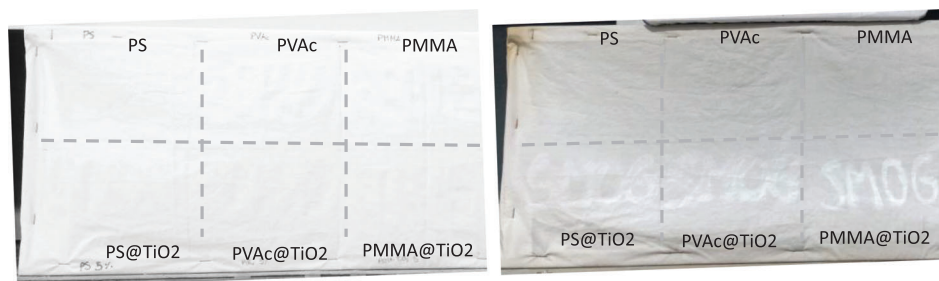

	PVAc@TiO$_2$	PMMA@TiO$_2$	PS@TiO$_2$
Homopolymer	**78.82° ± 3.19**	**80.22° ± 1.26**	**97.81° ± 1.75**
Nanocomposite	77.43° ± 1.21	80.12° ± 3.29	97.55° ± 1.10

Figure 12. The images show water droplets deposited on thin films of different nanocomposites. The measured contact angles are reported in the table.

Figure 13. Photos of canvas covered with thin films of homopolymers (top) and nanocomposites (bottom) just installed (image on the left) and exposed to air pollution for 9 months (image on the right).

5000 Versa Probe system (base pressure of the main chamber 1×10^{-8} Pa).[25a,31] Samples were excited with a Al-Kα X-ray radiation using a pass energy of 5.85 eV. Calibration was achieved by fixing the C 1s peak of the aliphatic carbon at 285.0 eV. The XPS peak intensities were obtained after Shirley's background removal.[25a,31] The atomic concentration analysis was performed by taking into account the relevant atomic sensitivity factors. The instrumental energy resolution was ≤ 0.5 eV.

Synthesis of Nanocomposites: The nanocomposites PMMA@TiO$_2$, PVAc@TiO$_2$, and PS@TiO$_2$ were produced through free radical bulk polymerization. Briefly, each monomer was purified through sodium sulfate and further basic alumina treatments. The purified monomer (1 g, $\approx$10 mmol) was then mixed with 50 mg of TiO$_2$ NPs, to obtain a final nanocomposite containing $\approx$5% (w) of the active photocatalyst. Each mixture was sonicated for 30 min before adding the AIBN initiator (17 mg, $\approx$0.1 mmol) within an 8 mL vial, and each mixture was kept in a heating bath at 55 °C for 20 h. Finally, the mixture was dissolved in THF (10 mL) and precipitated in *n*-hexane (60 mL). The nanocomposite was separated through filtration and dried in a vacuum oven (50 °C, 20 h).

The homopolymers PMMA, PVAc, and PS were synthesized using the same experimental procedure, without adding the TiO$_2$ NPs.

Preparation of Physical Mixtures: Physical mixtures of homopolymers (PMMA, PVAc, and PS) and TiO$_2$ NPs (obtaining the PMMA-TiO$_2$, PVAc-TiO$_2$, and PS-TiO$_2$ samples) were produced by mixing each homopolymer (95 mg) and TiO$_2$ NPs (5 mg) in THF (5 mL) and keeping the mixture in an ultrasonic bath for 30 min. Then, each obtained mixture was dried in a vacuum oven (50 °C, 20 h).

Thin Film Preparation for Raman Measurements: Each nanocomposite and blended mixture (1 mg) was dissolved in a CH$_2$Cl$_2$/Diethyl Ether mixture (1:1 v/v, 300 µL). A few drops of the solution were dropped onto a silicon plate and dried under nitrogen (24 h).

Photocatalytic Experiments: Thin films of each nanocomposite PMMA@TiO$_2$, PVAc@TiO$_2$, and PS@TiO$_2$ were prepared by dissolving $\approx$15 mg of each sample in THF (1.5 mL) and depositing the resulting solution on the inner wall of a glass test tube (150 mL). Particular care was taken to cover only 180° of the inner circumference, obtaining a final surface area of approximately 59 cm^2. Photocatalysis experiments were performed within an open-wall homemade apparatus, employing a solar lamp [OSRAM ultra vitalux (OSRAM Opto Semiconductors GmbH, Regensburg, Germany), Wattage 300 W, Radiated Power: (315–400 nm) 13.6 W, (280–315 nm) 3.0 W, Wavelength range 280–1000 nm] and a fan to cool the whole system. The test tube was fitted 30 cm from the lamp, onto a magnetic stirrer.

Each batch experiment involved dye aqueous solutions (100 mL), having appropriate concentration to start the photocatalytic test from absorbance values around 0.8 (Methylene Blue 10 µM, Rhodamine B 7 µM). The dye solutions were prepared using water (LC-MS grade) without any further degassing or aerating process.

A preliminary dark storage period (60 min) was performed under stirring to equilibrate the physical adsorption of the dye on the photocatalytic thin film. The system was then irradiated for 2 h under stirring (temperature 35 ± 1 °C).

The efficiency of the catalytic systems was examined by UV analysis of aliquots collected every 20 min (from C$_0$ to C$_{120}$) through UV-vis, monitoring the variations of the dye concentration (C/C$_0$) as a function of the reaction time, starting at the end of the dark-storage time ($t = 0$, C$_0$). Considering the pseudo-first-order photodegradation kinetic, the kinetic constant for the photodegradative process (k) is the linear fit slope of the ln(C/C$_0$) versus time plot.

Following the same procedure, photodegradation experiments of Paraquat and Acetaminophen in aqueous solutions ($\approx$80 µM) were performed.

Conflict of Interest

The authors declare no conflict of interest.

Data Availability Statement

The data that support the findings of this study are available from the corresponding author upon reasonable request.

[1] S. L. Lewis, M. A. Maslin, *Nature* **2015**, *519*, 171.

[2] G. Karthigadevi, S. Manikandan, N. Karmegam, R. Subbaiya, S. Chozhavendhan, B. Ravindran, S. W. Chang, M. K. Awasthi, *Bioresour. Technol.* **2021**, *324*, 124678.

[3] a) A. L. Power, R. K. Tennant, R. T. Jones, Y. Tang, J. Du, A. T. Worsley, J. Love, *New Front. Rare Earth Sci. Appl., Proc. Int. Conf. Rare Earth Dev. Appl.* **2018**, 6; b) M. Alexander, *Environ. Sci. Technol.* **2002**, 29, 2713; c) J. F. Davis, T. W. Kratzer, *Water Environ. Res.* **1997**, 69, 861.

[4] L. Pretali, F. Maraschi, A. Cantalupi, A. Albini, M. Sturini, *Catalysts* **2020**, 10, 628.

[5] J. Schneider, M. Matsuoka, M. Takeuchi, J. Zhang, Y. Horiuchi, M. Anpo, D. W. Bahnemann, *Chem. Rev.* **2014**, 114, 9919.

[6] S. Singh, H. Mahalingam, P. K. Singh, *Appl. Catal., A* **2013**, 462, 178.

[7] a) G. Žerjav, K. Žižek, J. Zavašnik, A. Pintar, *J. Environ. Chem. Eng.* **2022**, 10, 107722; b) M. Pelaez, N. T. Nolan, S. C. Pillai, M. K. Seery, P. Falaras, A. G. Kontos, P. S. M. Dunlop, J. W. J. Hamilton, J. A. Byrne, K. O'Shea, M. H. Entezari, D. D. Dionysiou, *Appl. Catal., B* **2012**, 125, 331; c) Y.-C. Nah, I. Paramasivam, P. Schmuki, *ChemPhysChem* **2010**, 11, 2698.

[8] C. M. Teh, A. R. Mohamed, *J. Alloys Compd.* **2011**, 509, 1648.

[9] S. A. Balsamo, R. Fiorenza, M. Condorelli, R. Pecoraro, M. V. Brundo, F. Lo Presti, S. Sciré, *Materials* **2021**, 14, 5938.

[10] a) L. Mezzina, A. Nicosia, F. Vento, G. De Guidi, P. G. Mineo, *Nanomaterials* **2022**, 12, 996; b) Q. Dai, J. Rabani, *New J. Chem.* **2002**, 26, 421.

[11] M. Wu, J. Jin, J. Liu, Z. Deng, Y. Li, O. Deparis, B.-L. Su, *J. Mater. Chem. A* **2013**, 1, 15491.

[12] R. Fiorenza, M. Bellardita, S. Scirè, L. Palmisano, *Mol. Catal.* **2018**, 455, 108.

[13] M. E. Fabiyi, R. L. Skelton, *J Photochem Photobiol A Chem* **2000**, 132, 121.

[14] M. Langlet, A. Kim, M. Audier, J. M. Herrmann, *J. Sol-Gel Sci. Technol.* **2002**, 25, 223.

[15] a) J. Xu, H. Nagasawa, M. Kanezashi, T. Tsuru, *ACS Omega* **2021**, 6, 1370; b) E. Halary-Wagner, F. Wagner, P. Hoffmann, *J. Electrochem. Soc.* **2004**, 151, c571.

[16] S. A. Elfeky, A.-S. A. Al-Sherbini, *Kinet. Catal.* **2011**, 52, 391.

[17] S. Naskar, S. Arumugom Pillay, M. Chanda, *J Photochem Photobiol A Chem* **1998**, 113, 257.

[18] A. Nicosia, F. Vento, G. M. Di Mari, L. D'Urso, P. G. Mineo, *Nanomaterials* **2021**, 11, 400.

[19] F. Vento, A. Nicosia, L. Mezzina, G. M. Rodríguez-Muñiz, M. A. Miranda, P. G. Mineo, G. De Guidi, *Chemosphere* **2022**, 303, 134988.

[20] A. Ballistreri, S. Foti, G. Montaudo, E. Scamporrino, *J. Poly. Sci.: Polym. Chem. Ed.* **1980**, 18, 1147.

[21] R. Zouzelka, J. Rathousky, *Appl. Catal., B* **2017**, 217, 466.

[22] a) Q. M. Al-Bataineh, A. A. Ahmad, A. M. Alsaad, A. D. Telfah, *Heliyon* **2021**, 7, e05952; b) I. S. Elashmawi, N. A. Hakeem, E. M. Abdelrazek, *Phys. B* **2008**, 403, 3547; c) J. E. Mark, *Polymer Data Handbook*, Oxford University Press, Oxford; New York **2009**.

[23] O. Frank, M. Zukalova, B. Laskova, J. Kürti, J. Koltai, L. Kavan, *Phys. Chem. Chem. Phys.* **2012**, 14, 14567.

[24] a) J. Wang, A. K. Mishra, Q. Zhao, L. Huang, *J. Phys. D: Appl. Phys.* **2013**, 46, 255303; b) V. Swamy, A. Kuznetsov, L. S. Dubrovinsky, R. A. Caruso, D. G. Shchukin, B. C. Muddle, *Phys. Rev. B* **2005**, 71, 184302.

[25] a) D. Briggs, J. T. Grant, *Surface Analysis by Auger and X-Ray Photoelectron Spectroscopy*, IM Publications, Chichester, West Sussex, UK **2003**; b) A. Gulino, A. E. Taverner, S. Warren, P. Harris, R. G. Egdell, *Surf. Sci.* **1994**, 315, 351.

[26] A. Gulino, G. G. Condorelli, I. Fragalà, R. G. Egdell, *Appl. Surf. Sci.* **1995**, 90, 289.

[27] H. R. Sadeghi, V. E. Henrich, *J. Catal.* **1988**, 109, 1.

[28] N. Kanth, W. Xu, U. Prasad, D. Ravichandran, A. M. Kannan, K. Song, *Nanomaterials* **2020**, 10, 1279.

[29] L. W. Miller, M. I. Tejedor-Tejedor, M. Perez Moya, R. Johnson, M. A. Anderson, *Stud. Surf. Sci. Catal.* **2000**, 130, 1925.

[30] A. H. Yuwono, J. Xue, J. Wang, H. I. Elim, W. Ji, Y. Li, T. J. White, *J. Mater. Chem.* **2003**, 13, 1475.

[31] A. Gulino, *Anal. Bioanal. Chem.* **2012**, 405, 1479.